Structural Integrity Facilitates Multi-Layer Modulation of the Brain-Metabolome-Microbiota Network by *Lilium lancifolium*-derived Vesicles in Depression

Na Li[1,#], Zhangfeng Zhong[2,#], Cuirong Wen[1], Ruipeng Shi[2], Fengyun Liao[2], Shuo Sang[1], Haochun Jin[2], Lili Zhang[2], Zhenlong Sun[1], Yuqiang Chen[1], Yuxuan Li[1], He Li[1], Pei Sun[3,*], Wen Tan[1,4,*]

1. *School of Pharmacy, Lanzhou University, Lanzhou 730000, China*
2. *Macao Centre for Research and Development in Chinese Medicine, State Key Laboratory of Quality Research in Chinese Medicine, Institute of Chinese Medical Sciences, University of Macau, Macao SAR 999078, China*
3. *Faculty of Health and Wellness, City University of Macau, Macao SAR 999078, China*
4. *State Key Laboratory of Natural Product Chemistry, Lanzhou University, Lanzhou 730000, China*

*Corresponding author:

Wen Tan: tanwen@lzu.edu.cn

Address: Lanzhou University, 199 Donggang Rd West, Lanzhou 730000, Gansu, China

Tel: (86) 0931 8915686

Pei Sun: peisun@cityu.edu.mo

Address: Faculty of Health and Wellness, City University of Macau, Macao SAR 999078, China

Tel: (853) 85902307

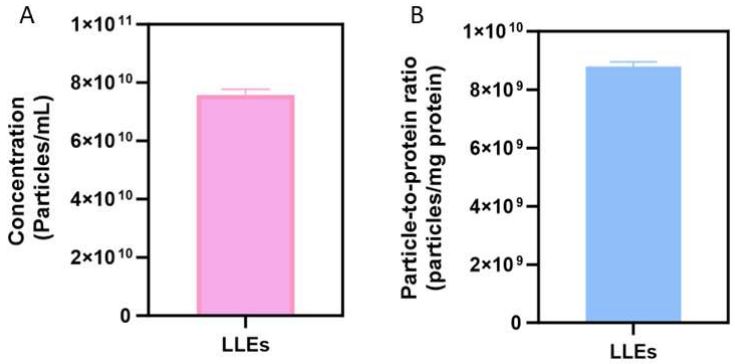

Fig. S1. Quantification of LLEs particle concentration and purity. (A) Particle concentration of purified LLEs (particles/mL) was determined by nanoparticle tracking analysis (NTA) using a ZetaView analyzer. **(B)** Particle-to-protein ratio (particles/mg protein), serving as an indicator of vesicle purity, was calculated by normalizing the NTA-derived particle concentration to the total protein content. Data are presented as mean ± SD (n = 3 independent biological batches).

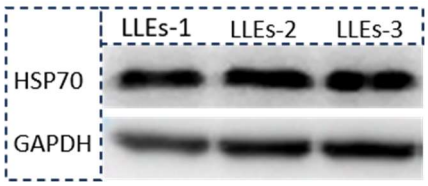

Fig. S2. Immunoblot validation of the candidate vesicle-associated protein HSP70 in LLEs. Representative Western blot images showing the robust presence of HSP70 protein across three independent biological preparations of LLEs. GAPDH was utilized as a loading control to ensure equal total protein input.

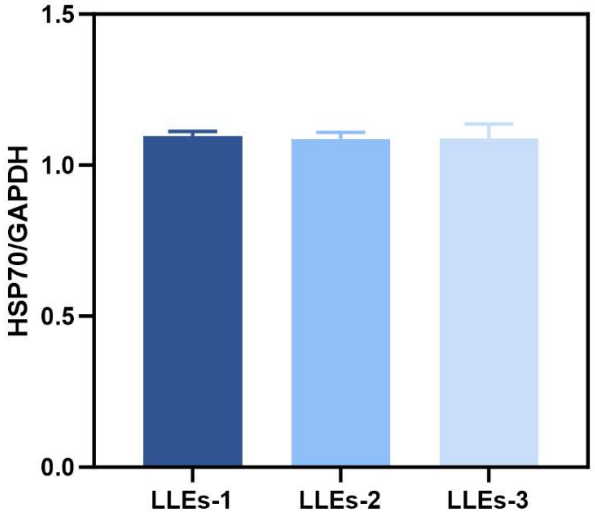

Fig. S3. Batch-to-batch consistency of HSP70 protein levels in LLEs. Western blot quantity of HSP70 in three independently prepared batches of LLEs (LLEs-1, LLEs-2, and LLEs-3). Densitometric analysis was performed by Image J analysis, with GAPDH serving as the internal loading control. The consistent HSP70/GAPDH ratios indicate the reproducible presence of HSP70 across independent preparations. Data are presented as mean ± SD (n = 3 independent batches).

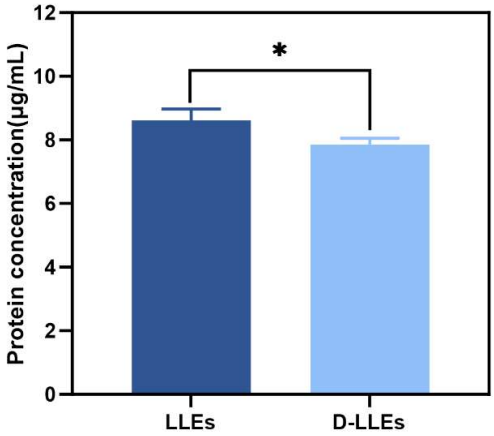

Fig. S4. Total protein quantification of intact LLEs and D-LLEs. LLEs were generated via Triton X-100-mediated membrane permeabilization followed by washing. Total protein concentrations of both intact LLEs and D-LLEs were subsequently measured using a BCA protein assay. While D-LLEs exhibited a modest but statistically significant reduction in protein concentration compared to intact LLEs, they retained a substantial portion of the total protein pool. Data are presented as mean ± SD (n = 3 independent biological preparations). *$p < 0.05$, as determined by Student's *t*-test.

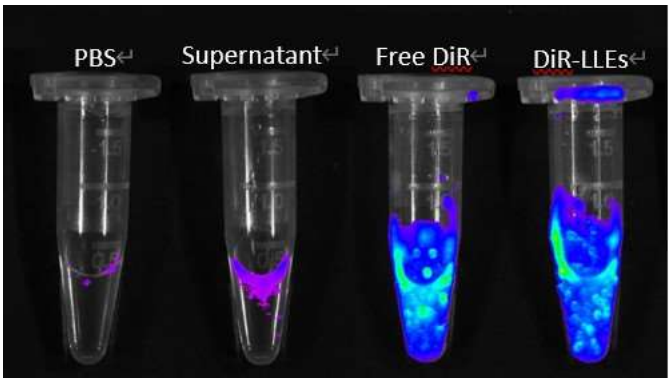

Fig. S5. Validation of DiR labeling efficiency and clearance of unbound dye. Representative images of PBS (negative control), the final wash supernatant, free DiR (positive control), and purified DiR-LLEs acquired under standardized fluorescence imaging parameters. The negligible signal in the final wash supernatant confirms the thorough elimination of unbound DiR during purification. Conversely, purified DiR-LLEs exhibit robust fluorescence, verifying successful labeling and ensuring signal specificity prior to *in vivo* biodistribution tracking.

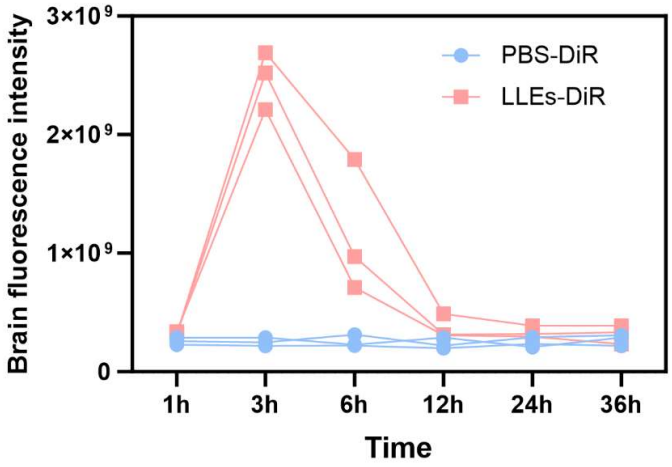

Fig. S6. Time-course quantification of brain fluorescence following DiR-LLEs administration. Brain fluorescence intensity was quantified *ex vivo* at 1, 3, 6, 12, 24, and 36 h post-administration of free DiR or DiR-LLEs. Compared to the free dye control, DiR-LLEs exhibited enhanced brain accumulation. The fluorescence signal of DiR-LLEs peaked rapidly at 3 h post-injection and maintained a sustained detectable presence through 6 h before gradual clearance. Fluorescence intensity is expressed as average radiance (p/s/cm²/sr).

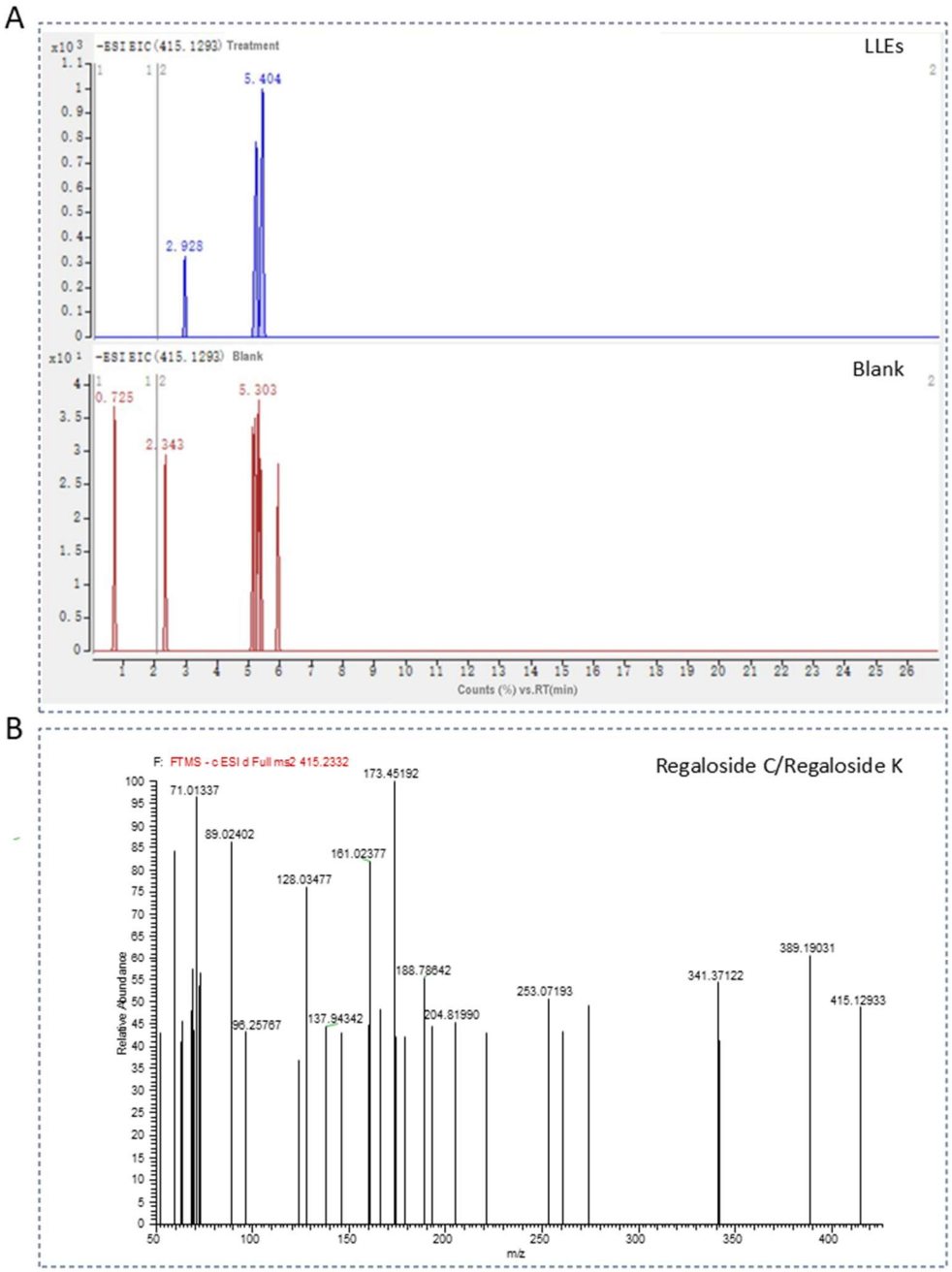

Fig. S7. Tentative LC-MS-based annotation of a Regaloside C/K-related feature in perfused brain tissue. (A) Representative extracted ion chromatograms (EICs) of the precursor ion at *m/z* 415.1293 ($[M-H]^-$) from LLEs-treated brain tissue and blank brain tissue. **(B)** MS/MS fragmentation spectrum of the *m/z* 415.1293 precursor ion. This feature was putatively assigned as a Regaloside C/K-related isomeric signal.

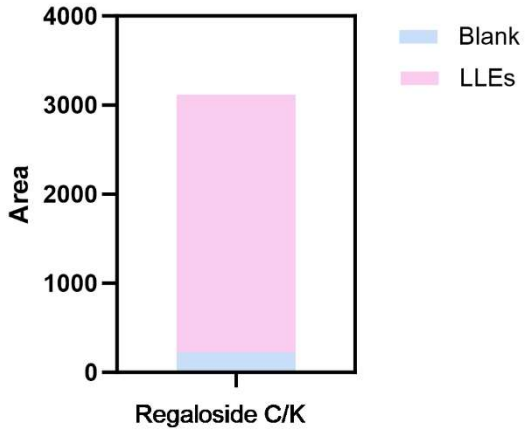

Fig. S8. Quantitative comparison of putative LLEs-associated small-molecule signals in brain tissue. Peak areas of Regaloside C/K -related signals were quantified in blank brain tissue and LLEs-treated brain tissue based on EIC. Brain-blank indicates blank brain matrix control; LLEs-brain indicates brain tissue collected after LLEs administration.

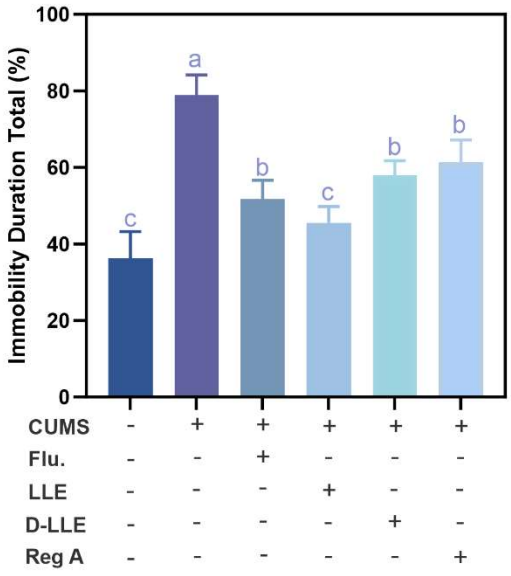

Fig. S9. LLEs attenuate CUMS-induced immobility in the open field test (OFT). The percentage of resting time during the OFT was quantified to evaluate anxiety-like behavior and baseline exploratory activity. CUMS exposure markedly increased the resting time compared to the control group. Treatment with Fluoxetine (Flu) or intact LLEs significantly attenuated this CUMS-induced immobility. In contrast, D-LLEs and Reg A exhibited only limited rescue effects. Data are presented as mean ± SD (n = 6

mice per group). Different lowercase letters (a, b, c, d) indicate statistically significant differences between groups ($p < 0.05$), as determined by one-way ANOVA followed by Tukey's post hoc test.

Supplementary Table 1

NO.	RT min	Ion mode	Measured m/z	Predicted m/z	Formula	Name	MS2	Error (ppm)
1	0.98	$[M-H]^-$	341.10849	341.10893	$C_{12}H_{22}O_{11}$	Sucrose	341.10849, 179.05550, 113.02374, 101.02377, 89.02381, 71.01330, 59.01336	-0.13
2	1.01	$[M+H]^+$	127.03898	127.03897	$C_6H_6O_3$	5-Hydroxymethylfurfural	127.03898, 109.02840, 81.03354, 69.03355, 53.03869	0.01
	1.23	$[M-H]^-$	125.02364	125.02442	C6H6O3	5-Hydroxymethylfurfural	125.02364, 97.02881, 69.03400	-0.62
3	1.33	$[M-H]^-$	134.04649	134.04722	$C_5H_5N_5$	Adenine	134.04649, 116.0665, 107.03556	-0.54
	1.4	$[M+H]^+$	136.06177	136.06177	$C_5H_5N_5$	Adenine	136.06177, 119.03519	0.00
4	1.4	$[M-H]^-$	191.01913	191.01973	$C_6H_8O_7$	Citric acid	191.01913, 111.00807, 87.00814, 85.02888	-0.31
5	1.55	$[M+H]^+$	268.10455	268.10403	$C_{10}H_{13}N_5O_4$	Adenosine	268.10455, 136.06181	0.19
6	1.59	$[M+H]^+$	252.10927	252.10912	$C_{10}H_{13}N_5O_3$	Cordycepin	252.10927, 136.06174	0.06
7	1.6	$[M-H]^-$	284.09985	284.09895	$C_{10}H_{13}N_5O_5$	Guanosine	284.09985, 152.05699	0.32

NO.	RT min	Ion mode	Measured m/z	Predicted m/z	Formula	Name	MS2	Error (ppm)
8	1.6	$[M+H]^+$	282.08401	282.08439	$C_{10}H_{13}N_5O_5$	Guanosine	282.08401, 150.04143, 133.01485	-0.14
9	2.62	$[M+H]^+$	166.08667	166.08626	$C_9H_{11}NO_2$	L-Phenylalanine	166.08667, 120.08101, 103.05442	0.25
	2.63	[M-H]-	164.07092	164.07170	$C_9H_{11}NO_2$	L-Phenylalanine	164.07092,147.04434, 72.00848	-0.48
10	4.3	$[M-H]^-$	341.10837	341.10893	$C_{12}H_{22}O_{11}$	Lactose	341.10837, 179.05542, 113.02372, 101.02373, 89.02377, 71.01328, 59.01332	-0.17
11	4.73	$[M-H]^-$	415.12933	415.12458	$C_{18}H_{24}O_{11}$	Regaloside C/Regaloside K	415.12933, 389.19031, 341.37122, 253.07193, 173.45192, 161.02377, 128.03477, 89.02402, 71.01337	1.14
12	4.91	$[M-H]^-$	/	353.08781	$C_{16}H_{18}O_9$	Chlorogenic acid	191.05544,173.04475, 135.04446	

NO.	RT min	Ion mode	Measured m/z	Predicted m/z	Formula	Name	MS2	Error (ppm)
13	4.98	$[M-H]^-$	399.12933	399.12967	$C_{18}H_{24}O_{10}$	Regaloside A/H	399.12933, 163.03935, 145.02878, 119.04949	-0.09
14	5.05	$[M-H]^-$	253.07135	253.07176	$C_{12}H_{14}O_6$	1-O-Caffeoylglycerol	253.07135, 179.03490, 161.02380, 148.10448, 135.04456	-0.16
15	5.13	$[M-H]^-$	/	337.09289	$C_{16}H_{18}O_8$	5-O-Coumaroylquinic acid	191.05548	
16	5.29	$[M-H]^-$	267.08701	267.08741	$C_{13}H_{16}O_6$	1-O-Feruloyglycerol	267.08701, 252.06345, 193.04988, 175.03944, 160.01599, 149.06013, 133.02881	-0.15
17	5.42	$[M-H]^-$	/	163.04007	$C_9H_8O_3$	3-Hydroxy-Cinnamic acid	162.83846, 119.04951, 92.99509	
18	5.47	$[M-H]^-$	193.05011	193.05063	$C_{10}H_{10}O_4$	Ferulic acid	193.05011, 178.02693, 134.03667	-0.27
19	5.84	$[M-H]^-$	/	753.40668	$C_{39}H_{62}O_{14}$	26-Hydroxymethyldiosgenin-triglucoside	205.07121, 163.06049, 143.03428, 101.02371, 89.02376, 59.01332	

NO.	RT min	Ion mode	Measured m/z	Predicted m/z	Formula	Name	MS2	Error (ppm)
20	6.08	$[M-H]^-$	/	443.13476	$C_{23}H_{24}O_9$	1,2-O-Di-feruloylcoumaroyglycerol	329.17920, 193.05009, 173.45178, 134.03662, 112.98492, 96.96896	
21	6.17	$[M-H]^-$	/	753.40668	$C_{39}H_{62}O_{14}$	25,27-Dihydroxyldiosgenin-diglucoside	205.07117, 163.06047, 143.03427, 101.02370, 89.02376, 59.01331	
22	6.22	$[M-H]^-$	/	737.41177	$C_{39}H_{62}O_{13}$	27-Hydroxyprosapogenin A	205.07126, 143.03427, 113.02373, 101.02373, 89.02378	
23	6.74	$[M-H]^-$	/	737.41177	$C_{39}H_{62}O_{13}$	Diosgenin-diglucoside	205.07115, 163.06049, 119.03428, 71.01327, 59.01333	
24	7.10	$[M-H]^-$	/	737.41177	$C_{39}H_{62}O_{13}$	Isodiosgenin-diglucoside	205.07123, 163.06053, 143.03429, 101.02374, 89.02379, 59.01334	
25	7.9	$[M-H]^-$	179.03479	179.03498	$C_9H_8O_4$	Caffeic acid	179.03479, 135.04463, 71.01328, 59.01335	-0.11

NO.	RT min	Ion mode	Measured m/z	Predicted m/z	Formula	Name	MS2	Error (ppm)
26	8.18	$[M-H]^-$	/	753.40668	$C_{39}H_{62}O_{14}$	27-Hydroxyl-diosgenin-maltoside	173.44915, 161.04491, 113.02367, 101.02375, 71.01328	
27	11.28	$[M-H]^-$	233.15472	233.15470	$C_{15}H_{22}O_2$	Curcumenol	233.15472	0.01
	11.28	$[M+H]^+$	235.16934	235.16926	$C_{15}H_{22}O_2$	Curcumenol	235.16934	0.04
28	12.23	$[M-H]^-$	137.02365	137.02442	$C_7H_6O_3$	4-Hydroxybenzoic acid	137.02365, 93.03387	-0.56

Supplementary Table 2

KEGG Enrichment of Model *vs.* Control (1)

Terms	Fold enrich	*p*.value	mapping
Biosynthesis of unsaturated fatty acids	3.18	0.00169	6
Linoleic acid metabolism	2.23	0.00523	9
Ether lipid metabolism	3.71	0.0716	2
Butanoate metabolism	2.12	0.086	4
Histidine metabolism	1.86	0.198	3
Phenylalanine, tyrosine and tryptophan biosynthesis	1.86	0.198	3
Propanoate metabolism	1.86	0.198	3
Ubiquinone and other terpenoid-quinone biosynthesis	1.86	0.198	3
Tryptophan metabolism	1.39	0.236	6
alpha-Linolenic acid metabolism	1.48	0.267	4
Tyrosine metabolism	1.59	0.283	3
Folate biosynthesis	1.86	0.294	2
Arginine biosynthesis	1.39	0.37	3
Fatty acid biosynthesis	1.48	0.409	2
Steroid hormone biosynthesis	1.48	0.409	2
Alanine, aspartate and glutamate metabolism	1.24	0.455	3

KEGG Enrichment of Model *vs.* Control (1)

β-Alanine metabolism	1.24	0.455	3
Lysine degradation	1.11	0.535	3
Pyrimidine metabolism	1.01	0.609	3
Arachidonic acid metabolism	0.93	0.674	3
Glyoxylate and dicarboxylate metabolism	0.93	0.674	3
Phenylalanine metabolism	0.93	0.674	3
Nicotinate and nicotinamide metabolism	0.93	0.685	2
Pantothenate and CoA biosynthesis	0.82	0.751	2
Glycerophospholipid metabolism	0.81	0.8	5
Glycine, serine and threonine metabolism	0.57	0.91	2
D-Amino acid metabolism	0.44	0.971	2
Cysteine and methionine metabolism	0.74	0.804	2

Supplementary Table 2 (continued)

KEGG Enrichment of LLEs *vs.* Model (2)

Terms	Fold enrich	*p*.value	mapping
Tyrosine metabolism	3.15	0.0215	4
Phenylalanine metabolism	2.3	0.0448	5
Citrate cycle (TCA cycle)	2.76	0.0742	3
Ubiquinone and other terpenoid-quinone biosynthesis	2.76	0.0742	3
alpha-Linolenic acid metabolism	2.21	0.0849	4
Butanoate metabolism	2.36	0.114	3
Pentose phosphate pathway	2.76	0.151	2
Glyoxylate and dicarboxylate metabolism	1.84	0.152	4
beta-Alanine metabolism	1.84	0.21	3
Pyruvate metabolism	2.21	0.224	2
Lysine degradation	1.65	0.264	3
Linoleic acid metabolism	1.47	0.278	4
Glutathione metabolism	1.84	0.298	2
Phenylalanine, tyrosine and tryptophan biosynthesis	1.84	0.298	2
Propanoate metabolism	1.84	0.298	2
Pyrimidine metabolism	1.5	0.319	3

KEGG Enrichment of LLEs *vs.* Model (2)

Terms	**Fold enrich**	***p*.value**	**mapping**
Tryptophan metabolism	1.38	0.324	4
Biosynthesis of unsaturated fatty acids	1.58	0.372	2
Nicotinate and nicotinamide metabolism	1.38	0.443	2
Alanine, aspartate and glutamate metabolism	1.23	0.509	2
Pantothenate and CoA biosynthesis	1.23	0.509	2
Arachidonic acid metabolism	0.92	0.677	2
Arginine and proline metabolism	0.92	0.677	2
D-Amino acid metabolism	0.65	0.854	2
Glycerophospholipid metabolism	0.48	0.95	2
Tyrosine metabolism	3.15	0.0215	4
Phenylalanine metabolism	2.3	0.0448	5
Arginine biosynthesis	1.38	0.443	2

Supplementary Table 3

Primer sequences of target genes used for RT-qPCR validation

Gene	NCBI Gene ID	Forward primer (5′→3′)	Reverse primer (5′→3′)
Gapdh	14433	CATCACTGCCACCCAGAAGACTG	ATGCCAGTGAGCTTCCCGTTCAG
Fasn	14104	CACAGTGCTCAAAGGACATGCC	CACCAGGTGTAGTGCCTTCCTC
Elovl5	68801	GGTGGCTGTTCTTCCAGATTGG	CTTCAGGTGGTCTTTCCTCCGA
Cyp2a5	13087	CCTTCCTCATCCGAATGCTGGA	TGACGGTCTCTGTGCCAGCAAA
Itgal	16408	CATGCAGCCTATCCTGAGACCT	GGTCAGGTTTGCCTCACACTTC